Applied Catalysis B: Environmental 165 (2015) 344–350

Contents lists available at ScienceDirect

Applied Catalysis B: Environmental

journal homepage: www.elsevier.com/locate/apcatb

On the improvement of PEC activity of hematite thin films deposited by high-power pulsed magnetron sputtering method

S. Kment[a,*], Z. Hubicka[b], J. Krysa[c], D. Sekora[d], M. Zlamal[c], J. Olejnicek[b], M. Cada[b], P. Ksirova[b], Z. Remes[b], P. Schmuki[e], E. Schubert[d], R. Zboril[a]

[a] Palacky University, RCPTM, Joint Laboratory of Optics, 17. listopadu 12, 771 46 Olomouc, Czech Republic
[b] Institute of Physics, Academy of Sciences of the Czech Republic, Na Slovance 2, 14800 Prague, Czech Republic
[c] Department of Inorganic Technology, Institute of Chemical Technology Prague, Technicka 5, 16628 Prague, Czech Republic
[d] Department of Electrical Engineering, University of Nebraska - Lincoln, Lincoln Nebraska 68588, USA
[e] Department of Materials Science and Engineering, University of Erlangen-Nuremberg, Martensstrasse 7, D-91058 Erlangen, Germany

ARTICLE INFO

Article history:
Received 13 July 2014
Received in revised form 3 October 2014
Accepted 6 October 2014
Available online 14 October 2014

Keywords:
Hematite
Very thin films
Photoelectrochemical water splitting
HiPIMS
ALD
Alumina passivation layer.

ABSTRACT

The work deals with fabrication of iron oxide (α-Fe_2O_3) hematite films by a novel high-power impulse magnetron sputtering method (HiPIMS). Hematite is regarded as a highly promising material for sustainable production of hydrogen via photoelectrochemical (PEC) water splitting. Some of the crucial issues of hematite are a large overpotential needed to develop the water oxidation photocurrent onset, high extent of surface defects acting as traps, and a short diffusion length (2–4 nm) of photogenerated holes. We report on minimizing these limits by deposition of highly photoactive nanocrystalline very thin (~30 nm) absorbing hematite films by HiPIMS and their passivation by ultra-thin (~2 nm) atomic layer deposited (ALD) isocrystalline alumina oxide (α-Al_2O_3) films. A new approach of one-step annealing of this bilayer system is introduced. The films were judged on the basis of physical properties such as crystalline structure, optical absorption, surface topography, and electronic properties. The functional properties were investigated under simulated photoelectrochemical (PEC) water-splitting conditions. The shift by 1 V vs. RHE and the maximal photocurrent value of 0.48 mA cm^{-2} at 1.23 V vs. RHE were achieved.

1. Introduction

Iron oxide (α-Fe_2O_3) in hematite crystalline structure has recently attracted much attention as possibly convenient material to be used for hydrogen production via photoelectrochemical (PEC) water splitting. It is due to its favorable properties such as a band gap between 2.0 and 2.2 eV, which allows absorbing a substantial fraction of solar spectrum, chemical stability in aqueous environment, nontoxicity, abundance, and low cost. For such band gap and assuming the standard solar illumination conditions (AM 1.5 G, 100 mW cm^{-2}) theoretical maximal solar-to-hydrogen (STH) conversion efficiency has been calculated at 15% [1].

On the other hand, hematite also possesses certain handicaps hindering to reach such high efficiency. Among the most cited limitations are [1–3]: (i) the nonideal position of hematite's conduction band, which is too low for spontaneous water reduction; (ii) the low absorptivity (especially for longer wavelengths) near its band-edge due to an indirect nature of the band gap; (iii) poor majority carriers concentration leading a low electrical conductivity and (iv) the penetration depth of photons in hematite is α^{-1} = 118 nm at λ = 550, however, due to extremely high bulk recombination rate (time constants in the range of 10 ps), the majority of the photogenerated holes undergo bulk recombination before reaching the semiconductor liquid junction (SCLJ), which causes very short diffusion length of the holes (L_D 2–4 nm) [4].

For each of these drawbacks, several more or less effective solutions have been proposed. The first limitation mentioned can be addressed by applying photovoltaic cell (e.g. dye-sensitized solar cell—DSSC) and/or a p-type semiconductor acting as the photocathode to provide the additional energy needed. In order to optimize solar photon harvesting, the cell can be placed on the top of hematite electrode or vice versa to work in a tandem ensuring that photons not absorbed by the first cell are transmitted to and subsequently absorbed by the second [5,6]. Doping with elements such as Sn, Ti, Si, Pt, etc. [7–10] can significantly increase the electronic conductivity by increasing the number of majority carriers' concentration. The negative effect of the short diffusion length of photogenerated holes can be suppressed by using very

* Corresponding author. Tel.: +420585634365; fax: +420585634958.
E-mail addresses: stepan.kment@upol.cz, kment@fzu.cz (S. Kment).

http://dx.doi.org/10.1016/j.apcatb.2014.10.015
0926-3373/

thin films of hematite or their careful nanostructuring in various dimensions and architectures (wormlike structure [11], nanorods [12], nanowires [13], etc.).

A large overpotential with respect to the flat band potential, V_{fb}, necessary to promote water oxidation is another key issue. For hematite Fe_2O_3, the flat band potential has been found to be around 0.5 V [1,14] versus the reversible hydrogen electrode (RHE). In the ideal case, the photocurrent is observed at all potentials more anodic than V_{fb}. The hematite, however, does not usually generate water oxidation photocurrent until the potential of 0.8–1.0 V vs. RHE [15]. Of course a certain external bias is consumed to suppress the energy deficit due to the aforementioned unsuitable energy level of the valance band. The remaining overpotential (0.5–0.6 V) has been attributed to two main reasons. The first one is the slow oxygen evolution reaction kinetics (OER), which has been addressed by anchoring various OER catalyst nanoparticles (IrO_2, Co–Pi, etc.) onto the hematite surface [15,16]. The second one suggests the presence of electronic surface states originated from oxygen vacancies and crystalline defects, which serve as traps for photogenerated holes. As a consequence, the so-called Fermi-level pining has been observed. The corundum isocrystalline oxide structures (Al_2O_3, Ga_2O_3, or In_2O_3) have been applied to effectively passivate these surface states and thus reduce the overpotential [17–19].

In this contribution, the attention was paid to the photoelectrochemical (PEC) processes with respect to the photogenerated holes. We clearly demonstrate the synergic effect of very thin nanocrystalline hematite films overlaid by passivating atomic layer deposition (ALD) Al_2O_3 ultra-thin (2 nm) coatings. This approach suppresses the negative impact of the short diffusion length of the holes, decrease the required overpotential for the photocurrent onset, and increase the overall current density value due to eliminating the charge backward recombination.

The hematite films were prepared by a novel low-temperature plasma deposition technique known as high-power impulse magnetron sputtering (HiPIMS). Generally, HiPIMS discharges work under pulse-modulated regime with a low repetition frequencies (typically about 100 Hz) and very short duty cycles (~1%), during which very high peak power powers are applied (~kW/cm^2) to the cathode (metal deposition target). A distinguishing feature of HiPIMS is its high degree of ionization of the sputtered metal and a high rate of molecular gas dissociation owing to very high plasma density near the target (order of 10^{13} ions cm^{-3}) [20,21]. This method is thus particularly convenient to implement the highly active hematite films in more complex and sophisticated 1D nanostructures (i.e. nanotubes) and the so-called host scaffold–guest absorber structures recently applied for PEC water splitting reactions. Such organizations provide a significant enhancement of the absorbed photon to current efficiency (APCE) due to a high surface area [22,23] simultaneously suppressing recombination of the holes in bulk.

Very thin hematite films demonstrating enhanced carrier collection and the APCE have been previously fabricated by spray pyrolysis [24] and ALD method [25]. Hisatomi et al. [24] demonstrated the maximum photocurrent density of 0.7 mA cm^{-2} at around 1.6 V vs. RHE and around 0.25 mA cm^{-2} at 1.23 V vs. RHE obtained by the system consisting of hematite (20 nm) electrode modified by an Nb_2O_5 underlayer (2.0 nm) and deposited at 520 °C. To the best of our knowledge, the combination of very thin hematite electrode and passivating overlayer has not been introduced yet.

2. Experimental

The preparation of hematite films was carried out in an ultra-high vacuum (UHV) chamber continuously pumped down by a combination of rotary and turbo-molecular pumps providing the base pressure of 10^{-5} Pa. The depositions were performed as the low-temperature HiPIMS reactive sputtering of pure iron target (99.995%, 50 mm outer diameter, Plasmaterials). Owing to a ferromagnetic behavior of the iron target, its thickness had to be reduced to 18 mm in order to ensure magnetic field of a sufficient intensity present at the surface of the magnetron target. The Ar–O_2 working gas mixture with the flow rates of 30 and 12 sccm (standard cubic centimeters per minute), respectively, was used. The operating pressure was 1 Pa. The average discharge current was always held constant on the value I_{AV} = 600 mA for the described experiments with HiPIMS magnetron. The pulsing frequency of HiPIMS discharge was varied in the range f_P = 70–1000 Hz and the "ON" time when the discharge was active was held on constant value T_{ON} = 100 μs and the maximal current density achieved in a pulse was 5 A cm^{-2} at 70 Hz. The distance between the magnetron target and the substrate was l_S = 60 mm. All these deposition conditions were kept constant during each deposition. The same technique has been used for photoactive hematite coating recently [26]. In that previous work, the ratio of ionized to neutral fluxes of depositing particles (parameter r) on the surface of substrate during hematite deposition was investigated. It was shown that the HiPIMS provides a high degree of ionization of sputtered particles (r = 0.44) for the highest pulse power applied (3.5×10^4 W). As the substrates carefully cleaned (combination of acetone, ethanol, and deionized water ultrasonic baths) transparent conductive fluorine-doped tin oxide (FTO, TCO-7, Solaronix) coated glass slides were applied. The HiPIMS deposition was carried at room temperature. However, a slight increase in the temperature of the substrate (~100 °C) can be expected owing to the sputtering process itself. The film thickness was measured by a set of techniques including optical ellipsometry, XPS, and SEM.

The depositions of Al_2O_3 overlayers were performed by means of Cambridge Nanotech–Fiji commercial ALD system. As the precursors , trimethylaluminum and water were used. The temperature raised up to 150 °C due to the ALD itself. Coatings consisted of 4 (~4 Å), 6 (~6 Å), 10 (~10 Å), and 20 (~20 Å) ALD cycles were compared. The ALD process was in-situ monitored by optical ellipsometry.

The crystalline phase of the Fe_2O_3 films was determined by Raman spectroscopy using Renishaw Raman Microscope RM 1000 (unpolarized beam in back scattering mode of a 514.5 nm Ar^+ laser). Optical properties were investigated by means of photothermal deflection spectroscopy (PDS) based on the deviation of the laser beam collinearly propagated with the sample surface [27]. The surface topography images were obtained with help of SEM (Hitachi S-520) and AFM (Thericroscopes). The 3D AFM scans served to estimate the surface RMS roughness.

The photoelectrochemical measurements were carried with help of a standard three-electrode arrangement, which has been previously applied for testing other photoresponding coatings [28,29]. In this configuration, the hematite-coated FTO substrate served as the working electrode, the Ag/AgCl (3 M KCl) introduced the reference electrode, and platinum plate was employed as the counter electrode. As the electrolyte, 1 M NaOH solution (pH 13.6) was used.

The measured potentials vs Ag/AgCl were converted to the reversible hydrogen electrode (RHE) scale according to the Nernst equation:

$$ER_{HE} = E_{Ag/AgCl} + 0.059pH + E^{\circ}_{Ag/AgCl}$$

where E_{RHE} is the converted potential vs. RHE, $E^{\circ}_{Ag/AgC}$ = 0.207 V at 25 °C, and $E_{Ag/AgCl}$ is the experimentally measured potential against Ag/AgCl reference. The Mott–Schottky characteristics were

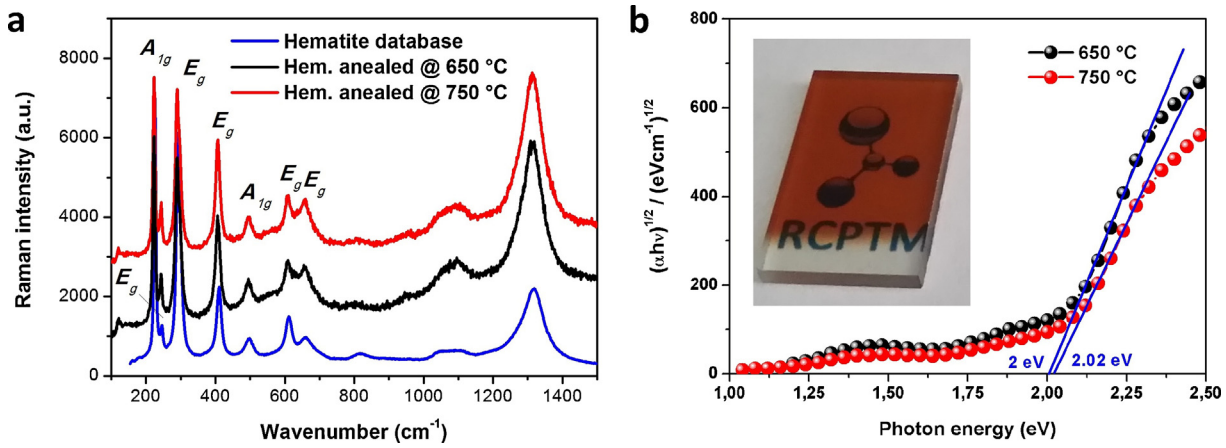

Fig. 1. HiPIMS-deposited Fe_2O_3 thin films annealed at 650 and 750 °C for 40 min: (a) Raman spectra and (b) the band gap energy width estimation based on Tauc analysis. Inset: the photograph of HiPIMS as-deposited film deposited onto FTO transparent substrate.

recorded using Zahner IM6 (Zahner Elektrik, Kronach, Germany). The measurements were performed under dark conditions at frequency of 500 Hz in 1 M NaOH electrolyte, with an amplitude of ±10 mV.

The time stability of the hematite photoanodes as well as the concentration of produced hydrogen were tested by the following set-up. A two-chamber glass cell with 1 M NaOH water solution working as the electrolyte was used. Anode and cathode chambers were separated by the glass frit to prevent mixing of the electrolyte. Potential of +1.5 V vs. RHE was applied to the sample (working electrode). Platinum sheet was applied as the counter-electrode. Each chamber was bubbled by argon gas (1 ml/min) separately. The illuminated area of the photoanode was 2 cm^2. The chambers were open to air by glass capillary to avoid mixing with air. Output gas from cathode chamber (platinum counter electrode) was analyzed by a gas chromatograph (Master, Dani) equipped with a plot column (Rt®-Msieve 5A, Restek) and a mTCD detector (Vici).

3. Results and discussion

3.1. Physical properties

The HiPIMS method was capable of reproducibly producing highly adherent iron oxide thin films. In our previous work, we have shown that the hematite crystalline structure can be obtained already during the deposition process although the temperature of the substrate does not exceed 150 °C [30]. This ability is a significant feature of the HiPIMS method. Regardless of this phenomenon, the films have to be annealed at elevated temperature in order to provoke interdiffusion of Sn from the FTO substrate into the hematite leading to Sn-doping. Besides increasing the donor density and thus the conductivity, the annealing also enhances the crystallinity itself and orderliness, which reduces the amount of the surface states and consequently the electron–hole pairs recombination [30]. In this study, two sets of bare hematite standards were prepared. Keeping the identical deposition conditions, the

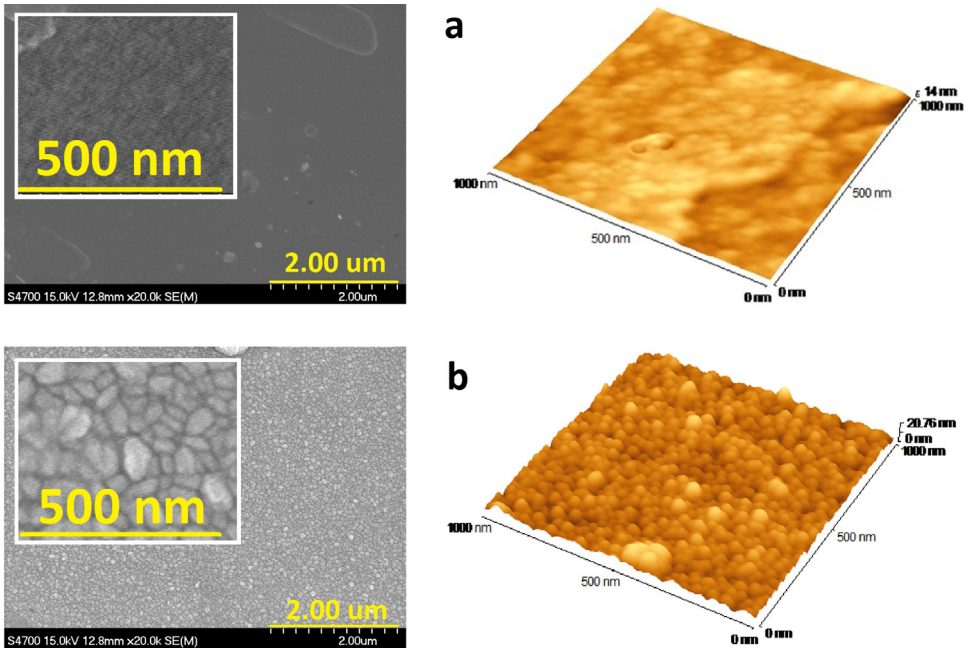

Fig. 2. Surface SEM (left column) and AFM (right column) images of hematite films: (a) films annealed at 650 °C and (b) films annealed at 750 °C, both for 40 min.

as-deposited hematite films were in the first case annealed at 650 °C and in the second at 750 °C always for 40 min. Fig. 1a shows the Raman spectra of the films prepared in this way. It is not observed a big difference between films calcinated at various temperatures. Both types exhibited only hematite Fe_2O_3 crystalline structure. The spectra show typical Raman bands of hematite, which are: A 1g (222 and 496 cm^{-1}), E g (242, 291, 408, and 610 cm^{-1}), and the 2-magnon scattering band at 1313 cm^{-1}. Fig. 1b depicts the optical band gap estimation based on the Tauc analysis of the absorption coefficient. Similarly, the temperature of the annealing did not cause a significant distinction of the optical characteristics since both types of films revealed the band gap energy around 2 eV, which is in the region of the tabulated values.

On the other hand, a certain difference was observed by examining surface morphology as it is seen from SEM and AFM images shown in Fig. 2. While the annealing at 650 °C led to very smooth surface of densely packed hematite nanoparticles, the increase of the temperature up to 750 °C initiated forming of slightly bigger grains obviously providing a higher surface area. This phenomenon was reflected also in the surface RMS roughness, which was assessed from AFM scans as 2 and 3.5 nm for 650 and 750 °C annealed films, respectively.

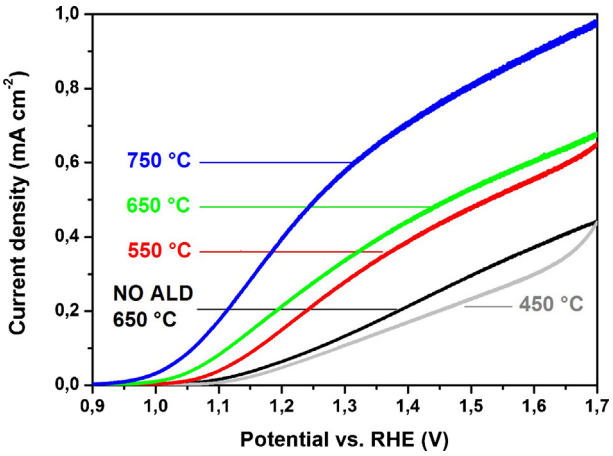

Fig. 3. Photoelectrochemical water-splitting activity of bare and ALD Al_2O_3 overlaid hematite films thermally treated at different temperatures. The bare (without ALD Al_2O_3 coating) hematite film annealed at 650 °C was used as the reference. The HiPIMS Fe_2O_3/ALD Al_2O_3 films were then annealed at 450, 550, 650, and 750 °C always for 40 min. The PEC characteristics were recorded under solar light AM 1.5 simulated conditions with the intensity of 100 mW cm^{-2}, using 1 M NaOH solution as the electrolyte, and with the scan rate 5 mV s^{-1}.

3.2. Photoelectrochemical water-splitting activity

Simulated PEC water-splitting activity was explored via the measurement of water oxidation photocurrent density as a function of applied potential under standard AM 1.5 (intensity 100 mW cm^{-2}) illumination. The polarization curves are presented in Fig. 3. Our preceding studies have demonstrated relatively high value of photocurrent density (0.45 mA cm^{-2} at 1.7 V vs. RHE) for very thin planar hematite films deposited by HiPIMS and annealed at 650 °C for 40 min [30]. Identically fabricated films representing the same physical properties as foreshown were used as the reference for this continuous work. These films, however, also undergo the typical weaknesses such as too anodic photocurrent onset potential at 1.09 V vs. RHE and thus relatively low water oxidation photocurrent density at 1.23 V (the thermodynamic potential for water splitting) vs. RHE of 0.08 mA cm^{-2} (see Fig. 3). In the next step, therefore, the as-deposited HiPIMS Fe_2O_3 films were coated with Al_2O_3 overlayers using the ALD technique. The number of 10 ALD coating cycles was kept the same for this type of experiment, which corresponded to the 1 nm thick Al_2O_3 film (calibrated by optical ellipsometry). Such prepared bilayer systems were then annealed at different temperatures (450, 550, 650, and 750 °C). This introduces other strategy than commonly used two-phase annealing, in which the as-prepared iron oxide films are calcinated first followed by the ALD coating and their subsequent thermal treatment. As it is evident from Fig. 3 when the bilayer system was annealed at 450 °C, the photocurrent values did not even reach the maxima of the bare hematite photoelectrode. This temperature level is probably still too low to improve the hematite crystallinity and more importantly owing to poor charge transfer among hematite particles themselves as well as between the FTO charge collecting substrate and the hematite film [31]. The polarization curve also showed more cathodic water oxidation dark current onset, which has been previously attributed to the photoelectrode imperfection such as inhomogeneity, low crystallinity, surface defect states, etc. After annealing at 550 °C, the photocurrent raised considerably but the applied overpotential remained almost unchanged. It emerges from this that the extent of surface photogenerated holes traps is effectively reduced. The increased photocurrent is hereupon a consequence of minimizing backward recombination of the charges. While the photogenerated holes still undergo, the slow OER kinetics reflected in the unshifted photocurrent onset.

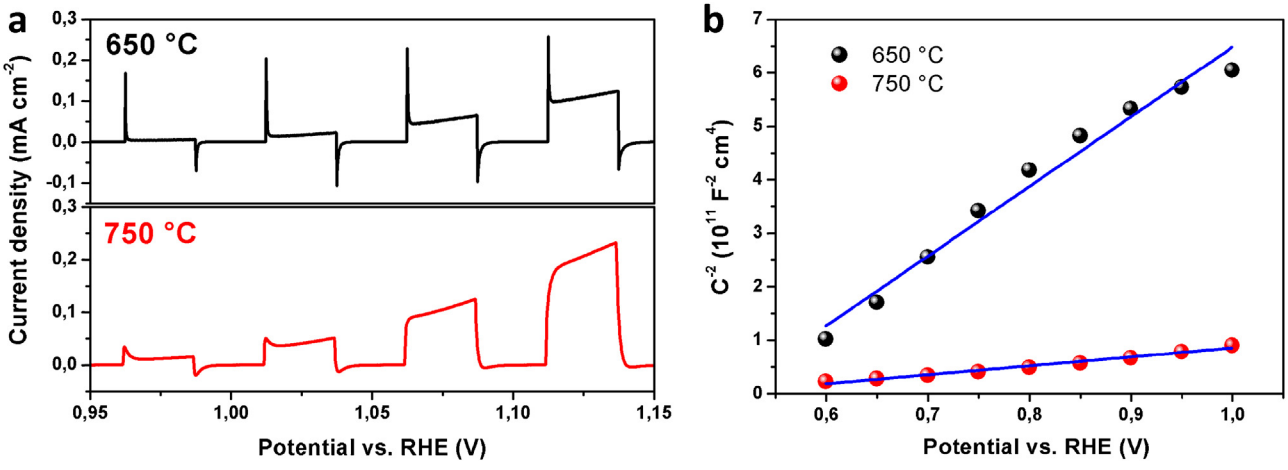

Fig. 4. Electrochemical characteristics of bare hematite films without ALD alumina passivation layer: (a) transient photocurrents measured under chopped light illumination (solar light AM 1.5, intensity 100 mW cm^{-2}) with periods of 5 s light/5 s dark; (b) Mott–Schottky plots of the films measured in dark, in 1 M NaOH electrolyte at frequency 500 Hz.

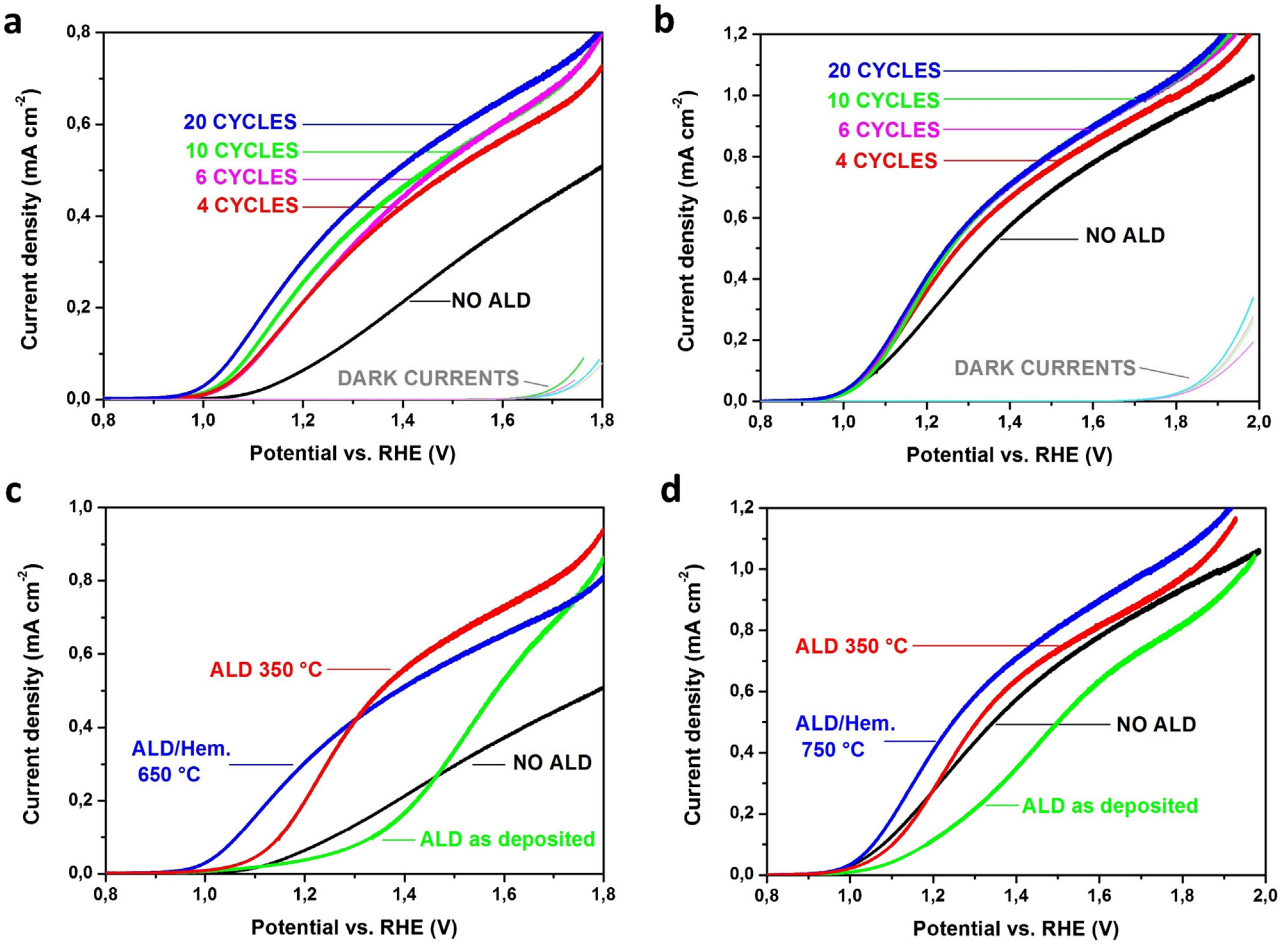

Fig. 5. PEC activity of the hematite films—the effect of ALD passivation Al_2O_3 overlayers: (1) the as-deposited hematite films annealed together with the as-deposited ALD Al_2O_3 overlayers—the effect of number of ALD coating cycles: (a) annealed at 650 °C/40 min; (b) annealed at 750 °C/40 min. (2) The annealing of as-deposited hematite prior to the ALD coatings—(c) as-deposited hematite annealed at 650 °C/40 min; (d) as-deposited hematite annealed at 750 °C/40 min. Photocurrent then measured with as-deposited ALD 2 nm alumina overlayers (green curve) and 2 nm ALD alumina overlayers annealed at 350 °C for 20 min (red curve). The blue curves represent the hematite/2 nm ALD alumina overlayers annealed at 650 and 750 °C for 40 min, respectively (reference). The PEC characteristics were recorded under solar light AM 1.5 simulated conditions with the intensity of 100 mW cm^{-2}, using 1 M NaOH solution as the electrolyte, and with the scan rate 5 mV s^{-1}. The dark current curves represent the polarization curves recorded without illumination.

Further increase in the annealing temperature to 650 and 750 °C led to the targeted polarization curves characteristics. Not only the overall photocurrent maxima were increased, but simultaneously their onset potential were also radically shifted catholically. Several favorable effects apparently contributed to this phenomenon. Firstly, the crystallinity of hematite is enhanced, meaning that more organized nanocrystals providing boosted charge transfer among the grain boundaries are developed. This assumption is supported by the SEM and AFM investigations and it is also in good agreement with other previously reported studies [4,31,32]. Secondly, less undesirable surface states are generated and these are further sufficiently passivate in a high extent by the ALD coatings. Consequently, the OER kinetics is improved and recombination of electron–hole pairs is eliminated. This is evident from the measurements of dynamic polarization curves of bare hematite films (without the alumina overlayers). The photocurrents displayed in Fig. 4 were recorded on the hematite films annealed at 650 and 750 °C for 40 min under the chopped light illumination. The effect of surface recombination is seen as the transient current response (the spikes) when the light is turned on and off. It has been proposed previously that the anodic current spikes are the consequence of the accumulated holes at the electrode/electrolyte interface. These holes are not injected to the electrolyte due to the slow water oxidation kinetics. On the contrary, they have ability to oxidize the trap states in the bulk as well as on the surface. Conversely, the cathodic transient spikes are generated upon the light-off, denoting the back recombination of the accumulated holes at the SCLJ by the electrons diffusing from the external circuit [18,33]. Since the extent of generation of the current spikes is much lower for the films annealed at 750 °C (Fig. 4a, the upper graph) also a lower concentration of the surface states can apparently be expected in case of these films. It significantly contributes to the enhanced overall PEC efficiency (see Fig. 3). Thirdly, one have to also take into consideration the doping of hematite by tin due to the thermally driven diffusion from FTO substrate, which increase the conductivity of hematite electrode. The presence of Sn in the films was verified by providing the XPS measurements data in our previous paper [30]. Additionally, the role of the Sn-doping was investigated by Mott–Schottky analysis as presented in Fig. 4b. From the plot of experimental capacitance data, C^{-2} as a function of applied potential V, the carrier density and flat band potentials can be assessed according to the Mott–Schottky equation [34] using the slope and intercept, respectively. Whereas the flat band potential of 0.5 V vs. RHE was the same for both types of the films, the donor densities of the hematite were calculated to be 1.35×10^{18} for 650 °C and 1.05×10^{19} cm^{-3} for 750 °C annealed hematite films. These data confirmed the increase in electron donors at higher temperature treatment owing to enhanced Sn-doping [35].

In the following experiments, the role of number of ALD cycles was scrutinized. Fig. 5a and b denotes the polarization curves recorded for 4, 6, 10 and 20 ALD coatings onto as-deposited iron oxide films, which correspond closest to 0.4, 0.6, 1 and 2 nm thin alumina overlayers, respectively. These systems were again annealed at 650and 750 °C for 40 min. The graphs also include dark polarization curves obtained without the films exposure by the light. In the case of layers (meaning the Al_2O_3/Fe_2O_3 assemblies) annealed at 650 °C, merely a slender shift of the photocurrent potential onset is seen with respect to the number of ALD alumina-coating cycles. The most apparently is shifted the system with 20 ALD cycles by 50–0.9 V vs. RHE comparing to rest of ALD-treated hematite films. It means that the maximum shift of the photocurrent onset potential achieved was by 100 mV from 1 to 0.9 V vs. RHE for the 650 °C annealed assembly of ALD Al_2O_3/HiPIMS Fe_2O_3. A substantially positive effect of the ALD passivation layers on the overall PEC activity characterized by the photocurrents is evident (see Fig. 5a). More than double increase of the photocurrent density was identified. Interesting features revealed the measurements of the bilayer system annealed at 750 °C. From Fig. 5b, it can be concluded that the ALD coatings did not influence the position of the photocurrent onset potential. The passivation of surface traps resulted only in slightly higher obtained photocurrents. However, if we compare the bare hematite coatings without the ALD treatment, the photocurrent onset is already for 750 °C annealed film shifted cathodically. Moreover, much higher photocurrent was achieved. One of the sources of the surface traps is the crystallinity imperfection. It seems that the calcination at the temperature level of 750 °C had a certain self-limiting effect towards the surface defects similarly to the work by Morrish et al. [36]. This finding corresponds well with afore-described photocurrent transient behavior, which revealed the less concentration of surface states for the hematite films thermally treated at 750 °C. The very high photocurrent achieved (0.48 mA cm^{-2}, at 1.23 V vs. RHE, 20 ALD alumina cycles) pushes these types of films among the champions of ultra-thin hematite photoelectrodes.

A different approach was next used. First, the reference hematite films were prepared by the annealing of as-deposited HiPIMS films at 650 and 750 °C analogously to previous experiments for 40 min. These films were overlaid by the alumina 20 cycles ALD coatings, which showed the best performance in the precious tests, and these were annealed once more at 350 °C for 20 min or left as-prepared. The photocurrent characteristics of these films are available in Fig. 5c and d, including the bare hematite films and the most active photoanodes previously identified for both temperatures used. It is clearly evident that the as-deposited alumina ALD coatings affected both reference hematite coatings strongly negatively. The reason is that the amorphous alumina films apparently suffer from a high degree of disorder inhibiting the hole injection from Fe_2O_3 into the electrolyte [18]. From the graphs, it can also be concluded that the simultaneous annealing of hematite and the ALD alumina passivation layers is more beneficial as always higher photocurrent at 1.23 V vs. RHE was reached. The presence of the alumina overlayer helps releasing the stress in the hematite films during the calcination and thus also much more minimizes the amount of defects than if the thermal treatments are separated [37].

The photocatalytic H_2 evolution was measured under simulated solar irradiation in 1 M NaOH electrolyte. Fig. 6 shows the time course for hydrogen evolution over hematite photoanodes with and without ALD passivation coatings. The results very well correspond to the preceding findings and discussions. We observed a similar stabilization stage as referred by Carraro et al. During this beginning period, an equilibrium of the evolving hydrogen in the PEC cell is established. Next, the PEC cell worked in a steady-state regime producing almost constant concentration of hydrogen over a long testing time. The highest concentration of evolved hydrogen was

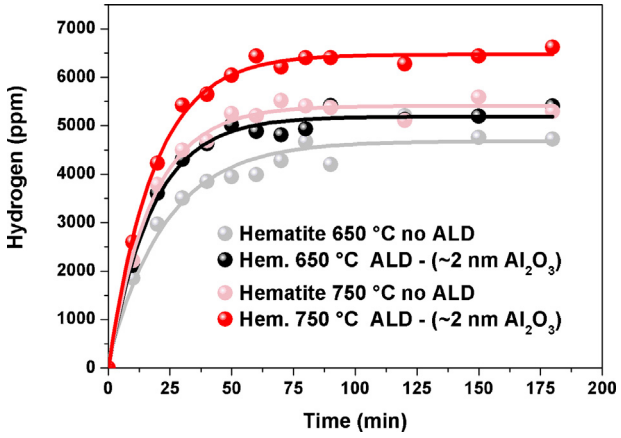

Fig. 6. Time course of hydrogen evolution using the bare hematite films annealed at 650 and 750 °C for 40 min and the hematite films coated by 20 ALD cycles (2 nm) of Al_2O_3 followed by the annealing at 650 and 750 °C as the photoanodes. The systems were illuminated by simulated solar light AM 1.5 with intensity 100 mW cm^{-2}, the applied potential to the photoanodes was 1.5 V vs. RHE, and the electrolyte was 1 M NaOH (pH ~ 13.6). The illuminated area of the photoanode was 2 cm^2.

achieved of the hematite photoanode annealed at 750 °C together with 2 nm (20 ALD cycles) Al_2O_3 overlayers. To the contrary, the lowest concentration of produced hydrogen was measured for bare hematite photoelectrode annealed at 650 °C. Moreover, this measurement proved the long-term stability of both untreated and treated hematite photoanodes. It is obvious that alumina was not dissolved in the electrolyte despite problematic thermodynamic stability at such high pH (~13.6 for 1 M NaOH). The scans lasted 3 h during which the hydrogen evolution remained highly stable.

4. Conclusion

The HiPIMS method was successfully applied for reactive deposition of photoactive very thin (~30 nm) hematite films. The as-deposited hematite films were annealed at 650 and 750 °C always for 40 min. The Raman spectra revealed only the hematite crystalline structure for both types. The band gap was estimated to be around 2 eV in both cases. Hematite films annealed at 750 °C showed more developed crystal grains and higher surface roughness. In order to increase the overall photoefficiency by suppressing the negative effect of surface states serving as the traps for photogenerated holes as well as by shifting the oxidation photocurrent onset potential more catholically the hematite films were overlayered by ultra-thin (0.4–2 nm) Al_2O_3 films using the ALD method. Several annealing steps were applied on these bilayer systems. We have demonstrated for the first time that the one annealing step of the as-deposited Fe_2O_3/as-deposited Al_2O_3 is more effective due to relaxation of the hematite film stress reducing the generation of the surface defects. The maximal shift of the photocurrent onset potential by 0.1 V vs. RHE was achieved for system of HiPIMS hematite/ALD (2 nm) alumina passivation layer annealed simultaneously at 650 °C for 40 min. On the other hand, the highest photocurrent value reached at 1.23 V vs. RHE was 0.48 mA cm^{-2} of the identical system but annealed together at 750 °C for 40 min.

Acknowledgements

This work was supported by the Grant Agency of the Czech Republic (project 13-29241P and project P108/12/2104), by the Operational Program Research and Development for Innovations - European Social Fund (project CZ.1.05/2.1.00/03.0058), Operational Program Education for Competitiveness - European Social Fund (project CZ.1.07/2.3.00/20.0017), and the project LD 12043 of the

Ministry of Education, Youth and Sports of the Czech Republic, and by National Science Foundation (USA) projects RII (EPS-1004094) and MRSEC (DMR-0820521).

References

[1] K. Sivula, F. Le Formal, M. Gratzel, ChemSusChem 4 (2011) 432–449.
[2] M.G. Walter, E.L. Warren, J.R. McKone, S.W. Boettcher, Q. Mi, E.A. Santori, N.S. Lewis, Chem. Rev. 110 (2010) 6446–6473.
[3] D.K. Bora, A. Braun, E.C. Constable, Energy Environ. Sci. 6 (2013) 407–425.
[4] K. Sivula, R. Zboril, F. Le Formal, R. Robert, A. Weidenkaff, J. Tucek, J. Frydrych, M. Grätzel, J. Am. Chem. Soc. 132 (2010) 7436–7444.
[5] M.T. Mayer, Ch. Du, D. Wang, J. Am. Chem. Soc. 134 (2012) 12406–12409.
[6] J. Brillet, J.H. Yum, M. Cornuz, T. Hisatomi, R. Solarska, J. Augustynski, M. Gratzel, K. Sivula, Nat. Photon. 6 (2012) 823–827.
[7] J. Frydrych, L. Machala, K. Tucek, K. Siskova, J. Filip, J. Pechousek, K. Safarova, M. Vondracek, J.H. Seo, O. Schneeweiss, M. Gratzel, K. Sivula, R. Zboril, J. Mater. Chem. **22**, (2012), 23232–23239.
[8] I. Cesar, K. Sivula, A. Kay, R. Zboril, M. Gratzel, J. Phys. Chem. C 113 (2009) 772–782.
[9] Y.S. Hu, A. Kleiman-Schwarsctein, A.J. Forman, D. Hazen, J.N. Park, E.W. McFarland, Chem. Mater. 20 (2008) 3803–3805.
[10] J. Liu, C.H. Liang, H.M. Zhang, Z.F. Tian, S.Y. Zhang, J. Phys. Chem. C 116 (2012) 4986–4992.
[11] J.Y. Kim, G. Magesh, D.H. Youn, J.W. Jang, J. Kubota, K. Domen, J.S. Lee, Sci. Rep.-UK 3 (2013) 2681, a. n.
[12] A. Mao, K. Shin, J.K. Kim, D.H. Wang, G.Y. Han, J.H. Park, ACS Appl. Mater. Int. 3 (2011) 1852–1858.
[13] L. Li, Y. Yum, F. Meng, Y. Tan, R.J. Hamers, J. Song, Nano Lett. 12 (2012) 724–731.
[14] K. Sivula, J. Phys. Chem. Lett. 4 (2013) 1624–1633.
[15] S. Tilley, M. Cornuz, F. Le Formal, J.H. Yum, M. Gratzel, Angew. Chem. Int. Ed. 49 (2010) 6405–6408.
[16] B. Klahr, S. Gimenez, F. Fabregat-Santiago, J. Bisquert, T.W. Haman, J. Am. Chem. Soc. 134 (2012) 16693–16700.
[17] T. Hisatomi, F. Le Formal, M. Cornuz, J. Brillet, N. Tetreault, K. Sivula, M. Gratzel, Energy Environ. Sci. 4 (2011) 2512–2515.
[18] F. Le Formal, N. Tetreault, M. Cornuz, T. Moehl, M. Gratzel, K. Sivula, Chem. Sci. 2 (2011) 737–743.
[19] M. Barroso, C.A. Mesa, S.R. Pendlebury, A.J. Cowan, T. Hisatomi, K. Sivula, M. Gratzel, D.R. Klug, J.R. Durrant, Natl. Acad. Sci. USA 109 (2012) 15640–15645.
[20] D. Lundin, K. Sarakinos, J. Mater. Res. 27 (2012) 780–792.
[21] M. Cada, P. Adamek, V. Stranak, S. Kment, J. Olejnicek, Z. Hubicka, R. Hippler, Thin Solid Films 549 (2013) 177–183.
[22] L. Wang, A. Palacios-Padros, R. Kirchgeorg, A. Tighineanu, P. Schmuki, ChemSusChem 7 (2014) 421–424.
[23] K. Sivula, F. Le Formal, M. Gratzel, Chem. Mater. 21 (2009) 2867.
[24] T. Hisatomi, H. Dotan, M. Stefik, K. Sivula, A. Rotchild, M. Gratzel, N. Mathews, Adv. Mater. 24 (2012) 2699–2702.
[25] B.M. Klahr, T.W. Hamann, J. Phys. Chem. C 115 (2011) 8393–8399.
[26] Z. Hubicka, S. Kment, J. Olejnicek, M. Cada, T. Kubart, M. Brunclikova, P. Ksirova, P. Adamek, Z. Remes, Thin Solid Films 549 (2013) 184–191.
[27] S. Kment, P. Kluson, Z. Hubicka, J. Krysa, M. Cada, I. Gregora, A. Deyneka, H. Zabova, L. Jastrabik, Electrochim. Acta 55 (2010) 1548–1556.
[28] S. Kment, P. Kluson, Z. Hubicka, J. Krysa, M. Cada, Electrochim. Acta 54 (2009) 3352–3359.
[29] M. Morozova, P. Kluson, J. Krysa, M. Zlamal, O. Solcova, S. Kment, T. Steck, J. Sol-gel Sci. Tech. 52 (2009) 398–407.
[30] S. Kment, Z. Hubicka, J. Krysa, J. Olejnicek, M. Cada, I. Gregora, M. Zlamal, M. Brunclikova, Z. Remes, N. Liu, L. Wang, R. Kirchgeorg, C.Y. Lee, P. Schmuki, Catal. Today 230 (2014) 8–14.
[31] X. Zong, S. Thaweesak, H. Xu, Z. Xing, J. Zou, G. Lu, L. Wang, Phys. Chem. Chem. Phys. 15 (2013) 12314–12321.
[32] D.K. Bora, A. Braun, S. Erat, O. Safonova, T. Graule, E.C. Constable, Curr. Appl. Phys. 12 (2012) 817–825.
[33] H. Dotan, K. Sivula, M. Grätzel, A. Rotshsild, S.C. Warren, Energy Environ. Sci. 4 (2011) 958–964.
[34] D.Ch. Bohn, A.K. Agrawal, E.C. Walter, M.D. Vaudin, A.A. Herzing, P.M. Haney, A.A. Talin, V.A. Szalai, J. Phys. Chem. C 116 (2012) 15290–15296.
[35] Y. Ling, G. Wang, D.A. Wheeler, J.Z. Zhang, Y. Li, Nano Lett. 11 (2011) 2119–2125.
[36] R. Morrish, M. Rahman, J.M. Don MacElroy, ChemSusChem 4 (2011) 274–479.
[37] D. Gan, P.S. Ho, Y. Pang, R. Huang, J. Leu, J. Maiz, T. Scherban, J. Mater. Res. 21 (2006) 1512–1518.